

**IFS DOCUMENTATION – Cy33r1**  
**Operational implementation 3 June 2008**

**PART V: ENSEMBLE PREDICTION  
SYSTEM**

**Table of contents**

**Chapter 1** Theory

**Chapter 2** Computational details: initial perturbations

**Chapter 3** Computational details: non-linear integrations

**References**

© Copyright 2009

European Centre for Medium-Range Weather Forecasts  
Shinfield Park, Reading, RG2 9AX, England

Literary and scientific copyrights belong to ECMWF and are reserved in all countries. This publication is not to be reprinted or translated in whole or in part without the written permission of the Director. Appropriate non-commercial use will normally be granted under the condition that reference is made to ECMWF. The information within this publication is given in good faith and considered to be true, but ECMWF accepts no liability for error, omission and for loss or damage arising from its use.



# Chapter 1

## Theory

### Table of contents

#### 1.1 Introduction

#### 1.2 Singular vectors

1.2.1 Formulation of the singular vector computation

1.2.2 Use of the total energy norm

1.2.3 Use of the Hessian of the 3D-Var objective function

#### Appendix A. Eigenvalue algorithms

A.1 The Lanczos algorithm

A.2 The Jacobi–Davidson algorithm

A.3 Solution method

### 1.1 INTRODUCTION

Ensemble prediction is a method to predict the probability distribution of forecast states, given a probability distribution of random analysis error and model uncertainties. In ensemble systems, the impact of analysis and model uncertainties on forecasts states are simulated by starting the ensemble of forecasts from different initial conditions, and computing each forecast evolution using schemes designed to simulate model uncertainties. Since 1992, ensemble prediction systems have been part of the operational forecasting suite at ECMWF (Palmer *et al.*, 1993) and NCEP (Toth and Kalnay, 1993, 1997). A general description of the first version of the ECMWF EPS can be found in Molteni *et al.* (1996), and a description of the current operational system is given by Leutbecher and Palmer (2008).

These implementations were followed in 1995 by MSC Canada (Houtekamer *et al.*, 1996b,a) and in 1998 by BMRC Australia. The reader is referred to Buizza *et al.* (2005) for a comparison of the performance of the ECMWF, MSC and NCEP ensemble systems over the northern hemisphere, and to Bourke *et al.* (2005) for a comparison of the performance of the ECMWF and the BoM systems over the southern hemisphere. In the past decade, other meteorological centres have started producing routinely ensemble-based probabilistic forecasts, see e.g. Park *et al.* (2008) for a very recent comparison of the performance of eight global ensemble prediction systems archived within the TIGGE project.

Since 12 September 2006, the ECMWF operational ensemble system has been running with a variable resolution (VAREPS, see Buizza *et al.* (2007) for a description of the system), with 51 members, one starting from unperturbed initial conditions (the control forecast) and 50 from perturbed initial conditions defined by adding small dynamically active perturbations to the operational analysis for the day. These 51 integrations are performed twice a day, with initial times 00 and 12 UTC, up to forecast day 15, with a (T399) resolution from day 0 to day 10, and with lower (T255) resolution from day 10 to day 15. In the vertical, all integrations have 62 levels, with the model top at 5 hPa.

Since 11 March 2008, the medium-range variable-resolution ensemble system (VAREPS) has been merged with the monthly coupled ensemble system, which has been operational at ECMWF since October 2004 (see Vitart (2004) for a description of the system). The merged VAREPS/monthly system (hereafter simply called the Ensemble Prediction System, EPS; see Vitart *et al.* (2008)) runs twice-a-day, at 00 and 12 UTC, with slightly different configurations:

- 00 UTC: forecasts are run with with persisted SST anomalies from day 0 to day 10, and with coupled ocean model from day 10 to day 15 every day apart for Thursday, when forecasts are extended to day 32.
- 12 UTC: forecasts are run with persisted SST anomalies from day 0 to day 15.

The ocean model is HOPE, the Hamburg Ocean Primitive Equation model (see [Wolff \*et al.\* \(1997\)](#)). This ocean model has lower horizontal resolution in the extra-tropics but higher horizontal resolution in the equatorial region, in order to resolve ocean baroclinic waves and processes. It has 29 vertical levels, and it is coupled to the atmospheric model through the Ocean Atmosphere Sea Ice Soil (OASIS, [Terray \*et al.\* \(1995\)](#)) coupler with a 3-hour frequency. The ocean initial conditions come from the near-real-time component of the operational ocean analysis (see [Balmaseda \*et al.\* \(2007\)](#)). To compute the ocean initial state at the beginning of LegB (day 9 in the current EPS configuration), for each ensemble member, the ocean model is integrated between day 0 and 9 using atmospheric fluxes from the atmosphere-only integration. Then, at day 9 the coupled LegB integration starts.

On 11 March 2008, a new ensemble re-forecast suite has been implemented to estimate the model climatological distribution (see [Hagedorn \(2008\)](#) for a description of the system). The re-forecast suite is based on 5-member ensembles, integrated with the same model version used in the operational EPS, and run once-a-week (on Thursdays) for the same calendar day over the past 18 years (in 2008, from 1990 to 2007). Thus, every week 90 ensemble members ( $5 \times 18$ ) can be accessed to estimate the model climatology and/or for further calibration purposes. The initial conditions for the re-forecasts are defined by ERA-40 analyses up to availability (July 2002), and then by operational analyses. Re-forecasts are used to generate some operational medium-range (e.g. the Extreme Forecast Index) and monthly products.

In these integrations, random model errors due to physical processes and subgrid-scale effects are represented by stochastically perturbing the tendencies of parameterized physical processes ([Buizza \*et al.\*, 1999b](#)). In situations where the ensemble is tightly distributed around the control integration, this forecast can be thought of as very likely to occur. More generally, the ensemble system gives a probability forecast of some given flow type, or some given category based on temperature, precipitation or other forecast variable. In other words, the ensemble system makes it possible not only to estimate the most likely scenario (e.g. the one given by the mean of all the ensemble forecasts), but also to estimate the probability of occurrence of weather scenarios of interest.

[Fig. 1.1](#) shows a schematic illustration of the phase-space evolution of the probability distribution function (PDF) of analysis error throughout the forecast range. A specific isopleth (e.g. the 1 standard deviation isopleth) is illustrated. It is assumed that at initial time the distribution is normal along each phase-space direction. At initial time ([Fig. 1.1\(a\)](#)), the isopleth is shown as isotropic, i.e. bounding an  $n$ -sphere, where  $n$  is the dimension of phase space ( $O(10^7)$ ) for the ECMWF operational forecast model). In general, this error will not be isotropic—analysis error is likely to be larger along directions which are less well observed, and vice versa. However, it is straightforward to define an inner product on phase space, with respect to which the initial probability density function (PDF) is isotropic. This inner product, defined from the analysis error covariance matrix, plays a fundamental role in the theory of singular vectors discussed below.

In the early part of the forecast, error growth is governed by linear dynamics. During this period an initially spherical isopleth of the PDF will evolve to bound an  $n$ -dimensional ellipsoidal volume ([Fig. 1.1\(b\)](#)). The major axis of the ellipsoid corresponds to a phase-space direction which defines the dominant finite-time instability of that part of phase space (relative to the analysis error covariance metric). The arrow shown in [Fig. 1.1\(b\)](#) points along the major axis of the ellipsoid. It can be thought of as evolving from the arrow shown in [Fig. 1.1\(a\)](#). Note that the arrows in [Fig. 1.1\(a\)](#) and [Fig. 1.1\(b\)](#) are not parallel to one another. This illustrates the non-modal nature of linear perturbation growth.

The arrows at initial and forecast time define the dominant singular vector at initial and final time (with respect to the analysis error covariance metric). At forecast time, the dominant singular vector defines the dominant eigenvector of the forecast error covariance matrix. See [Section 1.2.1](#) for more details.

The growth of the (isopleth of the) PDF between [Fig. 1.1\(b\)](#) and [Fig. 1.1\(c\)](#) describes a nonlinear evolution of the PDF. In [Figs 1.1\(c\)](#) the PDF has deformed from its ellipsoidal shape in [Fig. 1.1\(b\)](#). The nonlinear deformation will cause the PDF to evolve away from a normal distribution. Put another way, in the

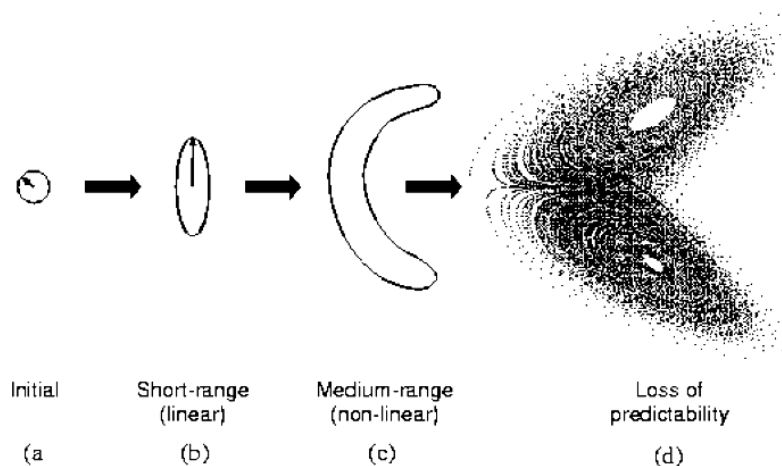


**Figure 1.1** A schematic illustration of the growth of an isopleth of the forecast error probability distribution function, from (a) initial phase, to (b) linear growth phase, to (c) nonlinear growth phase, to (d) loss of predictability. See text for further details.

nonlinear phase, the PDF in any given direction is partially determined by perturbations which, in the linear phase, were orthogonal to that direction. Finally, Fig. 1.1(d) shows (schematically) the situation where the evolved PDF has effectively become indistinguishable from the system's attractor, so that all predictability has been lost.

The number of degrees of freedom of the operational ECMWF model is (very) much larger than the largest practicable ensemble size. This raises the question of whether any particular strategy is desirable in sampling the initial PDF. If initial errors can occur independently in all the phase-space directions, then a strategy of random-under-sampling could lead to an EPS whose reliability was poor, especially for cases of small ensemble spread. In particular, if the spread from a randomly under-sampled ensemble was found to be small on a particular occasion, this could either be because the flow was especially predictable, or because the ensemble perturbations poorly sample the unstable subspace in which the analysis error lay. From a credibility perspective, it is important to try to minimize the latter type of occurrence.

An alternative strategy is to base the perturbations on the singular vectors. Clearly, by focusing on the unstable subspace, the cases of small spread being associated with large forecast error should be minimized, at least in the linear and weakly nonlinear range. In addition to this, there are five related reasons why the initial perturbations for the ECMWF EPS are based on the dominant singular vectors.

Firstly, as shown by Rabier *et al.* (1996), the sensitivity of day-2 forecast error to perturbations in the initial state projects well into the space of dominant singular vectors. Rabier *et al.* have shown that cases of severe forecast failure can be dramatically improved if the analysis is modified using the sensitivity perturbations.

Secondly, provided the metric or inner product for the singular vectors is an accurate reflection of the analysis error covariance matrix then, as mentioned, the evolved singular vectors point along the largest eigenvectors of the forecast error covariance matrix. As such (see Ehrendorfer and Tribbia, 1997), perturbations constructed from the dominant singular vectors represent the most efficient means for predicting the forecast error covariance matrix, given a pre-specified number of allowable tangent model integrations.

Thirdly, singular vector perturbations may provide a relatively efficient means of sampling the forecast error PDF in the nonlinear range, particularly during transitions in weather regimes. For example, Mureau *et al.* (1993) have shown a case where the singular vector perturbations were successful in capturing a major transition to blocking, where random perturbations were inadequate. Gelaro *et al.* (1998) have documented further such cases. A more systematic study of the ability of ensembles to describe the probability of regime transitions in the weakly nonlinear forecast range has been made by Trevisan *et al.* (2001) using an intermediate-complexity model of the extratropical circulation. Relatively small

ensembles initialised using firstly singular vectors, and secondly local Lyapunov vectors, were compared with a large Monte-Carlo ensemble based on random perturbations. It was found that small ensemble spread from the singular-vector ensemble was a reliable indicator of small ensemble spread from the Monte-Carlo ensemble. By contrast, small ensemble spread from the Lyapunov-vector ensemble was a much less reliable indicator of small spread from the Monte-Carlo ensemble.

Fourthly, in practice the initial PDF is only poorly known. Hence it is difficult to even define a truly random initial sampling.

Fifthly, from a purely pragmatic point of view, it would seem to be wasteful to integrate explicitly those perturbations that are likely to grow slowly, and thus resemble the control forecast. Such perturbations can be implicitly taken into account in constructing a forecast PDF, by increasing the weight given to the control forecast relative to the perturbed forecasts.

At present, the EPS is based on the notion that forecast uncertainty is dominated by error or uncertainty in the initial conditions (see [Harrison \*et al.\*, 1999](#)). This is consistent with studies that show that, when two operational forecasts differ, it is usually differences in the analyses rather than differences in model formulation that are critical to explaining this difference. In addition, random model errors due to physical parameterizations and the effects of subgrid-scale processes are represented by stochastic perturbations of the physical tendencies of the model, see [Buizza \*et al.\* \(1999b\)](#). The physical tendencies are multiplied with a random number between 0.5 and 1.5. Each ensemble member uses a different realization of this random number. The same perturbation is applied in a tile of  $10^\circ$  latitude and  $10^\circ$  longitude over a period of 6 time steps (i.e. 3 hours in the T399 integration and 4.5 hours in the T255 integration).

In the current system, each EPS perturbation is a linear combination of singular vectors with maximum growth computed using a total energy norm, over a 48 hour time period. 50 singular vectors are used for each extra-tropical hemisphere, and 5 singular vectors in each of up to 6 tropical areas are used, at T42 resolution and with 62 vertical levels. The assumption underlying the linear combination is that initial error is normally distributed in the space spanned by the singular vectors. A Gaussian sampling technique is used to sample realisations from this distribution (see [Leutbecher and Palmer \(2008\)](#) and [Section 2.4](#)).

The reader is referred to [Buizza and Palmer \(1995\)](#) for a description of the singular vector computation in the extra-tropics, and to [Barkmeijer \*et al.\* \(2001\)](#) for a discussion of the computation of the tropical singular vectors. The reader is also referred to [Palmer \*et al.\* \(1998\)](#) for a discussion of the sensitivity of the singular vector structure to the metric used to measure perturbation growth, to [Hoskins \*et al.\* \(2000\)](#) for an analysis of the nature of singular vector growth, and to [Barkmeijer \*et al.\* \(1998\)](#) for a comparison of singular vectors computed using a total energy or a Hessian metric.

## 1.2 SINGULAR VECTORS

### 1.2.1 Formulation of the singular vector computation

One way to define singular vectors is by means of a maximization problem. The scalar which has to be maximized can be written as

$$\frac{[\mathbf{E}\mathbf{M}\mathbf{x}, \mathbf{M}\mathbf{x}]}{[\mathbf{D}\mathbf{x}, \mathbf{x}]} \quad (1.1)$$

where  $[\cdot, \cdot]$  denotes the Euclidean inner product,  $[\mathbf{x}, \mathbf{y}] = \sum(x_i y_i)$ , and  $\mathbf{D}$  and  $\mathbf{E}$  are positive definite operators. The operator  $\mathbf{M}$  is the propagator of the tangent model. It assigns to a particular vector  $\mathbf{x}$  the linearly evolved vector  $\mathbf{M}\mathbf{x}$  for a given forecast time and with respect to a reference trajectory. Hence, the scalar defined by (1.1) is the ratio between the  $\mathbf{E}$ -norm of the evolved vector  $\mathbf{x}$  and the  $\mathbf{D}$ -norm of  $\mathbf{x}$  at initial time. Notice that the norm at initial and final time may differ. The leading singular vector has the property that it maximizes the scalar, the second singular vector maximizes the scalar in the space  $\mathbf{D}$ -orthogonal to the leading singular vector, and so forth. In this way, one obtains a set of singular vectors which are  $\mathbf{D}$ -orthogonal at initial time and  $\mathbf{E}$ -orthogonal at final time. The actual computation of the singular vectors in the IFS is done by solving an equivalent eigenvalue problem. Observe that the solutions of the maximization problem (1.1) also satisfy the generalized eigenvalue problem (1.2) given by

$$\mathbf{M}^* \mathbf{E} \mathbf{M} \mathbf{x} = \lambda \mathbf{D} \mathbf{x} \quad (1.2)$$

where  $\mathbf{M}^*$  is the adjoint of  $\mathbf{M}$ . The defining equation (1.2) can be generalized by activating operators in the singular vector computation, see Section 1.2. It is, for instance, possible to set the state vector to zero outside a prescribed area at optimization time, by using a projection operator  $\mathbf{P}$  Buizza (1994). Consequently, the growth of singular vectors outside the target area is not taken into account in the actual computation. In using this projection operator, the eigenvalue problem (1.2) becomes  $\mathbf{M}^* \mathbf{P}^* \mathbf{E} \mathbf{P} \mathbf{M} \mathbf{x} = \lambda \mathbf{D} \mathbf{x}$ . To keep the notation as simple as possible, these additional operators will be omitted from the basic eigenvalue problem (1.2).

The operator  $\mathbf{D}$  determines the properties by which the singular vectors are constrained at initial time. As such, it can be interpreted as an approximation of the inverse of the analysis error covariance matrix  $\mathbf{P}^a$ . Currently, there are two methods to compute singular vectors, depending on the form of  $\mathbf{D}$ . Both methods will be discussed in Subsections 1.2.2 and 1.2.3.

### 1.2.2 Use of the total energy norm

When using the total energy norm, or any other simple operator, at initial time, the generalized eigenvalue problem (1.2) can be simplified to an ordinary eigenvalue problem. In this case the  $\mathbf{D}$ -norm of  $\mathbf{x}$  reads as

$$[\mathbf{x}, \mathbf{D}\mathbf{x}] = \frac{1}{2} \int_0^1 \int_{\Sigma} \left\{ \Delta^{-1} \zeta_{\mathbf{x}} \cdot \zeta_{\mathbf{x}} + \Delta^{-1} D_{\mathbf{x}} \cdot D_{\mathbf{x}} + \frac{c_p}{T_{\text{ref}}} T_{\mathbf{x}}^2 + w_q \frac{L_{\text{cond}}}{c_p T_{\text{ref}}} q_{\mathbf{x}}^2 \right\} d\Sigma \frac{\partial p}{\partial \eta} d\eta + \frac{1}{2} \int_{\Sigma} R_{\text{dry}} T_{\text{ref}} P_{\text{ref}} \ln \pi^2 d\Sigma \quad (1.3)$$

where  $\zeta_{\mathbf{x}}$ ,  $D_{\mathbf{x}}$ ,  $T_{\mathbf{x}}$  and  $\ln \pi_{\mathbf{x}}$  stands for the vorticity, divergence, temperature, specific humidity and logarithm of the surface pressure component of the state vector  $\mathbf{x}$ , and  $c_p$  is the specific heat of dry air at constant pressure,  $L_{\text{cond}}$  is the latent heat of condensation at  $0^\circ\text{C}$ ,  $R_{\text{dry}}$  is the gas constant for dry air,  $T_{\text{ref}} = 300\text{ K}$  is a reference temperature and  $P_{\text{ref}} = 800\text{ hPa}$  is a reference pressure. The parameter  $w_q$  defines the relative weight given to the specific humidity term.

Since the operator  $\mathbf{D}$  is a diagonal matrix, one can easily define a matrix  $\mathbf{C}$  so that  $\mathbf{C}^2 = \mathbf{D}^{-1}$ . Multiplying both sides of (1.2) to the left and right with  $\mathbf{C}$ , yields the equation

$$\mathbf{C} \mathbf{M}^* \mathbf{E} \mathbf{M} \mathbf{C} \mathbf{x} = \lambda \mathbf{x} \quad (1.4)$$

which can be solved using the Lanczos algorithm, see Section A.1. The energy metric is believed to be a first-order approximation to the analysis error covariance metric (Palmer *et al.*, 1998).

### 1.2.3 Use of the Hessian of the 3D-Var objective function

In the incremental formulation of 3D-Var, the Hessian of the objective function  $\mathfrak{S}$  can be used as an approximation of the inverse of the analysis error covariance matrix. The objective function has the form

$$\mathfrak{S}(\delta\mathbf{x}) = \frac{1}{2} \delta\mathbf{x}^T \mathbf{B}^{-1} \delta\mathbf{x} + \frac{1}{2} (\mathbf{H} \delta\mathbf{x} - \mathbf{d})^T \mathbf{R}^{-1} (\mathbf{H} \delta\mathbf{x} - \mathbf{d}) \quad (1.5)$$

and the increment  $\delta\mathbf{x}^a$  where  $\mathfrak{S}$  attains its minimum, provides the analysis  $\mathbf{x}^a$  which is defined by adding  $\delta\mathbf{x}^a$  to the background  $\mathbf{x}^b$  so that

$$\mathbf{x}^a = \mathbf{x}^b + \delta\mathbf{x}^a \quad (1.6)$$

The operators  $\mathbf{B}$  and  $\mathbf{R}$  are covariance matrices of the background and observation error respectively and  $\mathbf{d}$  is the innovation vector given by

$$\mathbf{d} = \mathbf{y}^o - \mathbf{H} \mathbf{x}^b \quad (1.7)$$

where  $\mathbf{y}^o$  is the observation vector and  $\mathbf{H}$  is a linear approximation of the observation operator in the vicinity of  $\mathbf{x}^b$ .

The Hessian  $\nabla \nabla \mathfrak{S}$  of the objective function is given by

$$\nabla \nabla \mathfrak{S} = \mathbf{B}^{-1} + \mathbf{H}^T \mathbf{R}^{-1} \mathbf{H} \quad (1.8)$$

Provided that the background error ( $\mathbf{x}^b - \mathbf{x}^t$ ) and the observation error ( $\mathbf{y}^o - \mathbf{H} \mathbf{x}^t$ ) are uncorrelated, with  $\mathbf{x}^t$  the true state of the atmosphere, the Hessian  $\nabla \nabla \mathfrak{S}$  is equal to the inverse of the analysis error

covariance matrix  $\mathbf{P}^a$ . This follows by noting that the objective function is quadratic and attains its unique minimum at  $\delta\mathbf{x}^a$  and consequently, by using (1.6),

$$\mathbf{B}^{-1}[\mathbf{x}^a - \mathbf{x}^t - (\mathbf{x}^b - \mathbf{x}^t)] + \mathbf{H}^T \mathbf{R}^{-1}[\mathbf{H}(\mathbf{x}^a - \mathbf{x}^t) + \mathbf{H}\mathbf{x}^t - \mathbf{y}] = 0 \quad (1.9)$$

Rewriting (1.9) gives

$$(\mathbf{B}^{-1} + \mathbf{H}^T \mathbf{R}^{-1} \mathbf{H})(\mathbf{x}^a - \mathbf{x}^t) = \mathbf{B}^{-1}(\mathbf{x}^b - \mathbf{x}^t) - \mathbf{H}^T \mathbf{R}^{-1}(\mathbf{H}\mathbf{x}^t - \mathbf{y}) \quad (1.10)$$

Using the assumption that the background and observation error are uncorrelated the above equation implies that

$$(\mathbf{B}^{-1} + \mathbf{H}^T \mathbf{R}^{-1} \mathbf{H})\mathbf{P}^a(\mathbf{B}^{-1} + \mathbf{H}^T \mathbf{R}^{-1} \mathbf{H})^T = (\mathbf{B}^{-1} + \mathbf{H}^T \mathbf{R}^{-1} \mathbf{H})^T \quad (1.11)$$

Now by multiplying each side of (1.11) to the right with its transpose, the desired result follows.

The defining eigenvalue problem for the singular vectors becomes

$$\mathbf{M}^* \mathbf{E} \mathbf{M} \mathbf{x} = \lambda \nabla \nabla \mathfrak{S} \mathbf{x} \quad (1.12)$$

Since the objective function is quadratic in the incremental formulation, the Hessian  $\nabla \nabla \mathfrak{S} \mathbf{x}$  in (1.12) can be evaluated as finite difference of two gradients:  $(\nabla \nabla \mathfrak{S}) \mathbf{x} = \nabla \mathfrak{S}(\mathbf{x} + \mathbf{x}^b) - \nabla \mathfrak{S}(\mathbf{x}^b)$ . The generalized eigenvalue problem (1.12) is solved by using the Jacobi–Davidson algorithm, see Section A.2.

## APPENDIX A. EIGENVALUE ALGORITHMS

### A.1 The Lanczos algorithm

Algorithms based on Lanczos theory are very useful to solve an eigenvalue problem when only a few of the extreme eigenvectors are needed. It can be applied to large and sparse problems. The algorithm does not access directly the matrix elements of the operator that defines the problem, but it gives an estimate of the eigenvectors through successive application of the operator.

Consider the eigenvalue problem

$$\mathbf{A} \mathbf{x} = \sigma_i^2 \mathbf{x} \quad (A.1)$$

where the matrix  $\mathbf{A}$  is  $N \times N$  dimensional, and symmetric. Without loss of generality, we can also suppose that it is real.

If  $\mathbf{A}$  is a real, symmetric matrix, then there exists an orthogonal real matrix  $\mathbf{Q}$  such that

$$\mathbf{Q}^T \mathbf{A} \mathbf{Q} = \mathbf{D}(\lambda_1, \dots, \lambda_N) \quad (A.2)$$

where  $\mathbf{D}(\lambda_1, \dots, \lambda_N)$  is a diagonal matrix, and  $\mathbf{Q}^T$  denotes the transpose of  $\mathbf{Q}$  (Schur decomposition theorem).

The Lanczos algorithm does not directly compute the diagonal matrix  $\mathbf{D}$ , but it first computes a partial transformation of the matrix  $\mathbf{A}$  using a tridiagonal matrix  $\mathbf{T}$

$$\mathbf{Q}^T \mathbf{A} \mathbf{Q} = \mathbf{T} \quad (A.3)$$

with

$$\mathbf{T} = \begin{bmatrix} \alpha_1 & \beta_2 & 0 & \cdot & \cdot & \cdot & \cdot \\ \beta_2 & \alpha_2 & \beta_3 & 0 & \cdot & \cdot & \cdot \\ 0 & \beta_3 & \cdot & \cdot & \cdot & \cdot & \cdot \\ \cdot & 0 & \cdot & \cdot & \cdot & 0 & \cdot \\ \cdot & \cdot & \cdot & \cdot & \cdot & \beta_{J-1} & 0 \\ \cdot & \cdot & \cdot & 0 & \beta_{J-1} & \alpha_{J-1} & \beta_J \\ \cdot & \cdot & \cdot & \cdot & 0 & \beta_J & \alpha_J \end{bmatrix} \quad (A.4)$$

and with

$$\mathbf{Q} = [\mathbf{q}_1, \dots, \mathbf{q}_J] \quad (A.5)$$



where the vectors  $\mathbf{q}_j$  are column vectors, and where the number of iterations  $J$  is much smaller than the dimensionality of the problem,  $J \ll N$ . Then, the Lanczos algorithm finds the diagonal decomposition of  $\mathbf{T}$

$$\mathbf{T} = \mathbf{S}^T \mathbf{D} \mathbf{S} \quad (\text{A.6})$$

The elements of the diagonal matrix  $\mathbf{D}$  are an estimate of the eigenvalues of  $\mathbf{A}$ , and an estimate of the eigenvectors are given by  $\mathbf{Y} = [\mathbf{y}_1, \dots, \mathbf{y}_j]$ , with

$$\mathbf{Y} = \mathbf{Q} \mathbf{S} \quad (\text{A.7})$$

The actual computation is performed by writing (A.3) as

$$\mathbf{A} \mathbf{Q} = \mathbf{Q} \mathbf{T} \quad (\text{A.8})$$

Equating columns of (A.8), it follows that

$$\mathbf{A} \mathbf{q}_j = \beta_{j-1} \mathbf{q}_{j-1} + \alpha_j \mathbf{q}_j + \beta_j \mathbf{q}_{j+1} \quad (\text{A.9})$$

for  $j = 1, \dots, J$ . The orthogonality of the vectors  $\mathbf{q}_j$  implies that

$$\alpha_j = \mathbf{q}_j^T \mathbf{A} \mathbf{q}_j \quad (\text{A.10})$$

Moreover, if

$$\mathbf{r}_j = (\mathbf{A} - \alpha_j \mathbf{I}) \mathbf{q}_j - \beta_{j-1} \mathbf{q}_{j-1} \quad (\text{A.11})$$

is non-zero, then

$$\mathbf{q}_{j+1} = \frac{\mathbf{r}_j}{\beta_j} \quad (\text{A.12})$$

where  $\beta_j = \pm \sqrt{\langle \mathbf{r}_j; \mathbf{r}_j \rangle}$ . An iterative application of these equations, with a randomly chosen starting vector  $\mathbf{q}_1$ , defines the Lanczos iterative procedure. The total number of iterations  $J$  determines the accuracy of the computation. As this number increases, more eigenvalues/eigenvectors can be separated from the others, independently from the choice of the starting vector  $\mathbf{q}^T$ . This separation starts from the boundaries of the eigenvalue spectrum. The accuracy of the eigenvectors is less than the accuracy of the singular values, say to order  $\varepsilon$  when the precision of the singular values is of order  $\varepsilon^2$ .

The reader is referred to [Golub and van Loan \(1983\)](#) for a theoretical description of the Lanczos algorithm. The Lanczos code is available in NAG issue 17.

## A.2 The Jacobi–Davidson algorithm

The generalized eigenproblem

$$\mathbf{A} \mathbf{x} = \lambda \mathbf{B} \mathbf{x} \quad (\text{A.13})$$

is usually handled by bringing it back to a standard eigenproblem

$$\mathbf{B}^{-1} \mathbf{A} \mathbf{x} = \lambda \mathbf{x} \quad (\text{A.14})$$

The matrix  $\mathbf{B}^{-1} \mathbf{A}$  is in general nonsymmetric, even if both  $\mathbf{A}$  and  $\mathbf{B}$  are symmetric. However, if  $\mathbf{B}$  is symmetric and positive definite, the  $\mathbf{B}$ -inner product is well defined. The matrix  $\mathbf{B}^{-1} \mathbf{A}$  is symmetric in this inner product if  $\mathbf{A}$  is symmetric:

$$[\mathbf{w}, \mathbf{B}^{-1} \mathbf{A} \mathbf{v}]_{\mathbf{B}} = [\mathbf{B} \mathbf{w}, \mathbf{B}^{-1} \mathbf{A} \mathbf{v}] = [\mathbf{w}, \mathbf{A} \mathbf{v}] = [\mathbf{A} \mathbf{w}, \mathbf{v}] = [\mathbf{B}^{-1} \mathbf{A} \mathbf{w}, \mathbf{v}]_{\mathbf{B}} \quad (\text{A.15})$$

The proposed method to solve (A.14) constructs a set of basis vectors  $\mathbf{V}$  of a search space  $v$ , c.f. the Lanczos method. The approximate eigenvectors are linear combinations of the vectors  $\mathbf{V}$ . The classical and most natural choice for the search space  $v$ , for instance utilized in the Lanczos method, is the so-called Krylov subspace, the space spanned by the vectors

$$\mathbf{v}, \mathbf{B}^{-1} \mathbf{A} \mathbf{v}, (\mathbf{B}^{-1} \mathbf{A})^2 \mathbf{v}, \dots, (\mathbf{B}^{-1} \mathbf{A})^{i-1} \mathbf{v} \quad (\text{A.16})$$

This  $i$ -dimensional subspace is denoted by  $\mathbf{K}^i(\mathbf{v}, \mathbf{B}^{-1}\mathbf{A})$ . The vector  $\mathbf{v}$  is a starting vector that has to be chosen. The Krylov subspace is well suited for computing dominant eigenpairs since the vector  $(\mathbf{B}^{-1}\mathbf{A})^{i-1}\mathbf{v}$  points more and more in the direction of  $\mathbf{B}^{-1}\mathbf{A}$  the dominant eigenvector of for increasing  $i$ .

Given a search space  $v$ , the approximate eigenpair  $(\theta, \mathbf{u})$  of (A.15) is a linear combination of the basis vectors of  $v$  so that

$$\mathbf{u} = \mathbf{V}\mathbf{y} \quad (\text{A.17})$$

A suitable criterion for finding an optimal pair is the Galerkin condition that the residual

$$\mathbf{r} = \mathbf{B}^{-1}\mathbf{A}\mathbf{u} - \theta\mathbf{u} = \mathbf{B}^{-1}\mathbf{A}\mathbf{V}\mathbf{y} - \theta\mathbf{V}\mathbf{y} \quad (\text{A.18})$$

is  $\mathbf{B}$ -orthogonal to the search space to  $v$ . Hence

$$\mathbf{V}^T\mathbf{B}\mathbf{r} = 0 \quad (\text{A.19})$$

and consequently, using (A.19),

$$\mathbf{V}^T\mathbf{A}\mathbf{V}\mathbf{y} - \theta\mathbf{V}^T\mathbf{B}\mathbf{V}\mathbf{y} = 0 \quad (\text{A.20})$$

Note that the resulting eigenproblem is of the dimension of the search space, which is generally much smaller than of the original problem. The basis vectors are usually orthogonalized so that  $\mathbf{V}^T\mathbf{B}\mathbf{V} = \mathbf{I}$ . Approximate eigenpairs that adhere to the Galerkin condition are called Ritz pairs.

It can be shown that the residuals  $\mathbf{r}_1, \mathbf{r}_2, \dots, \mathbf{r}_i$  form a  $\mathbf{B}$ -orthogonal basis for  $\mathbf{K}^i(\mathbf{r}_1, \mathbf{B}^{-1}\mathbf{A})$  when the approximate eigenpairs are computed according to (A.17).

### A.3 Solution method

As was stated before, the natural search space for the generalized eigenvalue problem is the Krylov subspace  $\mathbf{K}^i(\mathbf{v}, \mathbf{B}^{-1}, \mathbf{A})$ . This basis can be generated by expanding the basis by new residual vectors. The problem in the construction of a basis for this space is that operations with  $\mathbf{B}^{-1}$  are needed. Since in our application the inverse of  $\mathbf{B}$  is not known explicitly, its action is approximated by the Conjugate Residual method (CR). To compute the vector

$$\mathbf{r} = \mathbf{B}^{-1}\tilde{\mathbf{r}} \quad (\text{A.21})$$

one iteratively solves the system

$$\mathbf{B}\mathbf{r} = \tilde{\mathbf{r}} \quad (\text{A.22})$$

Iterative solution methods require, apart from vector operations, only multiplications with  $\mathbf{B}$ . The vector  $\mathbf{r}$  can in principle be determined to high accuracy. This, however, may require many multiplications with  $\mathbf{B}$  and hence may be very expensive. Therefore, the action of  $\mathbf{B}^{-1}$  is approximated to low accuracy, by performing only a few steps with an iterative solution method. The number of iterations is controlled by NINNER. The subspace generated in this way is not a Krylov subspace and the basis vectors are not the residuals (A.19) but only approximations to it. As a consequence they are not perfectly  $\mathbf{B}$ -orthogonal. This has to be done explicitly.

The complete algorithm can be summarized as follows.

- (i) Choose a starting vector  $\mathbf{v}$ .
- (ii) Compute  $\mathbf{B}\mathbf{v}$ ,  $\mathbf{B}$ -normalize  $\mathbf{v}$ .
- (iii) Repeat the (iv) to (x) steps NITERL times.
- (iv) Compute  $\mathbf{A}\mathbf{V}$ ,  $\mathbf{V}^T\mathbf{A}\mathbf{V}$
- (v) Solve small eigenproblem  $\mathbf{V}^T\mathbf{A}\mathbf{V}\mathbf{y} = \theta\mathbf{y}$ .
- (vi) Select Ritz value  $\theta$  and  $\mathbf{y}$ .
- (vii) Compute Ritz vector  $\mathbf{u} = \mathbf{V}\mathbf{y}$  and residual  $\tilde{\mathbf{r}} = \mathbf{A}\mathbf{V}\mathbf{y} - \theta\mathbf{B}\mathbf{V}\mathbf{y}$ .
- (viii) Compute approximately  $\mathbf{v} = \mathbf{B}^{-1}\tilde{\mathbf{r}}$  with the CR-method.
- (ix)  $\mathbf{B}$ -orthonormalize new  $\mathbf{v}$  against  $\mathbf{V}$ .
- (x) Expand  $\mathbf{V}$  with the resulting vector.

The matrix  $\mathbf{V}$  contains the basis for the search space, the vector  $\mathbf{v}$  contains the new basis vector and  $(\mathbf{u}, \theta)$  is an approximate eigenpair. In step (vi) the pair with the largest  $\theta$  is selected because the dominant part of the spectrum is only of interest. However, if the eigenpair approximation reaches a certain accuracy  $\varepsilon$  (XKAPA in namelist NAMLCZ), i.e.,  $\tilde{\mathbf{r}} = \mathbf{A}\mathbf{u} - \theta\mathbf{B}\mathbf{u} \leq \varepsilon$ , a smaller  $\theta$  is selected. In step (viii) a few CR steps are performed to approximate the action of  $\mathbf{B}^{-1}$ . In step (ix), the Modified Gram–Schmidt procedure is used for reasons of numerical stability. For a more detailed description of the Jacobi–Davidson algorithm the reader is referred to [Sleijpen and van der Vorst \(1996\)](#)



## Chapter 2

# Computational details: initial perturbations

### Table of contents

|            |   |
|------------|---|
| <b>2.1</b> | <b>Introduction</b>                                     |
| <b>2.2</b> | <b>The singular vector code</b>                         |
| 2.2.1      | Set-up routines   |
| 2.2.2      | Main routines   |
| <b>2.3</b> | <b>Computation of singular vectors</b>                  |
| 2.3.1      | Extra-tropical singular vectors                         |
| 2.3.2      | Singular vectors targeted on tropical cyclones          |
| <b>2.4</b> | <b>Calculation of initial perturbations</b>             |
| <b>2.5</b> | <b>Unperturbed analysis retrieval and interpolation</b> |
| <b>2.6</b> | <b>Analysis error estimate retrieval and smoothing</b>  |
| <b>2.7</b> | <b>Generation of initial perturbations</b>              |
| 2.7.1      | Standard deviation for Gaussian sampling                |
| 2.7.2      | Gaussian sampling coefficients                          |
| 2.7.3      | Linear combination                                      |
| <b>2.8</b> | <b>Generation of the perturbed initial conditions</b>   |

## 2.1 INTRODUCTION

For a description of the evolution of the ECMWF Ensemble Prediction System (EPS) the reader is referred to [Molteni \*et al.\* \(1996\)](#), [Buizza \*et al.\* \(1998, 1999a, 2003, 2007\)](#) and [Leutbecher and Palmer \(2008\)](#). As mentioned in [Section 1.1](#), for each initial date, an ECMWF ensemble comprises one ‘control’ forecast, which is a forecast started from the operational analysis, and  $N_{\text{ens}}$  perturbed forecasts. The initial conditions for the perturbed integrations are constructed by adding and subtracting to the operational analysis  $N_{\text{ens}}/2$  perturbations obtained from the leading singular vectors through a Gaussian sampling technique ([Leutbecher and Palmer, 2008](#)). The sampling uses the leading 50 singular vectors of each of the following four sets of singular vectors:

- (i) Initial northern hemisphere singular vectors, file ‘svifs’.
- (ii) Evolved northern hemisphere singular vectors, file ‘svevo’.
- (iii) Initial southern hemisphere singular vectors, file ‘svifss’.
- (iv) Evolved southern hemisphere singular vectors, file ‘svevos’.

In addition, the sampling uses the leading 5 singular vectors from each of up to 6 sets of singular vectors which are optimised for specific tropical depressions/cyclones, files ‘svifs1’ to ‘svifs6’ ([Puri \*et al.\*, 2001](#)). These singular vectors are computed with a diabatic tangent-linear model ([Barkmeijer \*et al.\*, 2001](#)).

## 2.2 THE SINGULAR VECTOR CODE

The singular vector computation is called from `CUN3` in `CNT0` or from `CUN2` in `CUN1`, depending on whether the Hessian of the objective function is used or not. General routines related to the singular vector computation can be found in the directory ‘sinvect’. The technical routine needed for the Lanczos and Jacobi–Davidson algorithms is contained in the directory ‘var’ of IFS.

### 2.2.1 Set-up routines

Details of the set-up routines are given in [Table 2.1](#).

### 2.2.2 Main routines

The defining equation for the singular vectors (1.2) takes the form

$$\text{OPK}(\mathbf{x}) = \lambda \text{OPM}(\mathbf{x}) \quad (2.1)$$

The routine **OPM** is the identity in case a simple energy norm is used at initial time, or it is equal to the Hessian of the 4D-Var objective function. In the routine **OPK**, the propagators of the tangent and adjoint model are evaluated. Depending on the setting of the constants in **NAMLCZ**, additional operators may be active, such as **SPTRLCZTL** when **LSPTRLC0** = TRUE. It truncates the state vector in spectral space by setting all harmonic coefficients with total wavenumber smaller than **NWTRMIN0**, or larger than **NWTRMAX0**, to zero at initial time.

## 2.3 COMPUTATION OF SINGULAR VECTORS

The computation of singular vectors for the EPS is organised in the following tasks in family (/mc/main/HH/sv). Task names are given in parentheses.

- (i) Retrieval of the 6-hour forecast from the which is used to initialise the singular vector trajectory (**getini**).
- (ii) Interpolation of the forecast to T42L62, the resolution of the singular vectors (**inidata\_sv**).
- (iii) Computation of the extra-tropical initial singular vectors for the Southern (**svsh**) and Northern Hemisphere (**svnh**).
- (iv) Optimisation regions for the singular vector computations targeted on tropical cyclones are determined (**targets**).
- (v) Definition of the subspace of extra-tropical singular vectors used when computing the singular vectors targeted on a tropical cyclone (**subspace**).
- (vi) Computation of up to six sets of singular vectors targeted on tropical cyclones (**sv1**), (**sv2**), ... (**sv6**).
- (vii) Computation of the evolved singular vectors for the Northern (**svnhevo**) and Southern Hemisphere (**svshevo**).

At the time of revising this documentation (July 2007), the singular vector resolution is T42L62.

The nonlinear trajectory which defines the tangent-linear system is started from a 6-hour forecast from the delayed-cutoff stream. The use of a slightly less accurate trajectory does not significantly alter the singular vector structure and does not compromise the probabilistic skill of the EPS ([Leutbecher, 2005](#)). It has the advantage that more resources can be devoted to the singular vector computation and that the nonlinear forecasts can be started as soon as the final analysis is available.

### 2.3.1 Extra-tropical singular vectors

For each hemisphere, the leading 50 singular vectors are computed. The tangent-linear model uses an adiabatic version of the forecast model (apart from vertical diffusion and surface friction).

### 2.3.2 Singular vectors targeted on tropical cyclones

Initial EPS perturbations in the tropics are included since cycle Cy24r3 (introduced operationally in January 2002). The leading 5 singular vectors are computed in each of up to 6 target areas. Each tropical depression/storm (WMO class  $\geq 1$ ) reported on the GTS is potentially assigned its own optimisation region. When the tropical depression/storm could be tracked in the EPS run 12 hours before the initial time, the track information is used to determine the optimisation region; otherwise the optimisation region is centred on the reported position of the tropical storm. When the procedure generates more than 6 target regions the regions that overlap the most or are closest to each other are merged. In addition, regions with a very large overlap are merged. If no tropical storm is present in the Caribbean region an additional

**Table 2.1** Constants in namelist *NAMLCZ* controlling the singular vector computation. Defaults refer to *LECMWF=TRUE*.

| Name           | Type    | Purpose  | Default  |
|----------------|---------|--|--|
| LANCZOS        | LOGICAL | Activates singular vector computation with Lanczos algorithm (NCONF = 601)   | TRUE   |
| LJACDAV        | LOGICAL | Activates singular vector computations with Jacobi–Davidson algorithm (NCONF = 131)  | FALSE  |
| L_USE_CONGRAD  | LOGICAL | Use Lanczos algorithm in subroutine <b>CONGRAD</b>   | TRUE   |
| LOCNORM        | LOGICAL | Switch to localize norm computation in grid space  | TRUE   |
| ALAT1          | REAL    | } NW corner of local area (defined by point 1)   | 90.0   |
| ALON1          | REAL    |  | 0.0  |
| ALAT3          | REAL    |  | } SE corner of local area (defined by point 3) |
| ALON3          | REAL    | 359.9  |  |
| NLEVMIN        | INTEGER | Minimum level of local area  | 1  |
| NLEVMAX        | INTEGER | Maximum level of local area  | NLEVG  |
| LSPTRLC0       | LOGICAL | Switch to truncate in spectral space at initial (0) time   | FALSE  |
| LSPTRLC1       | LOGICAL | Switch to truncate in spectral space at final (1) time   | FALSE  |
| NWTRMIN0(1)    | INTEGER | Spectral coefficients with total wavenumber outside window are set to zero   | 0  |
| NWTRMAX0(1)    | INTEGER |  | NXMAX  |
| LNEWNORMT0     | LOGICAL | Switch to re-define the norm at initial time   | FALSE  |
| NEWNORMT0      | INTEGER | Re-defines initial norm<br>1: total energy<br>2: kinetic energy<br>3: vorticity squared<br>4: stream function squared<br>5: rotational kinetic energy  | 1  |
| NITERL         | INTEGER | Maximum number of Lanczos or Jacob–Davidson inner iterations   | 70   |
| NWEIGL         | INTEGER | Number of singular vectors that are requested  | 50   |
| XKAPA          | REAL    | Relative accuracy of RITZ value to consider a singular vector as converged   | 0.01   |
| XMIN_RITZ      | REAL    | Smallest accepted RITZ value in <b>CONGRAD</b>   | 1.0  |
| NINNER         | INTEGER | Number of Jacobi–Davidson inner iterations   | 2  |
| NJDSTOP        | INTEGER | Value of NSTOP when LJACDAV = TRUE   | 144  |
| LEVOLC         | LOGICAL | Switch to evolve singular vectors  | TRUE   |
| NEIGEVO        | INTEGER | Number of singular vectors to evolve   | 35   |
| NLANTYPE       | INTEGER | Determines type of singular vectors<br>1: energy type norms are used<br>2 and 3: obsolete<br>4: same as 1 but now NCONF = 131<br>5: Hessian is used at initial time<br>6: for computing eigensystem of the Hessian | 1  |
| LSYMCHECK      | LOGICAL | Switch to activate symmetry test for operator OPK  | FALSE  |
| L_SUBSPACE_SVS | LOGICAL | Compute singular vectors in subspace orthogonal to first N_DIM_SUBSPACE vectors in file 'sv_subspace'  | FALSE  |
| N_DIM_SUBSPACE | INTEGER | Number $N_{\text{sub}}$ of vectors in 'sv_subspace' used to define subspace  |  |
| LSCALC         | LOGICAL | Write inner product coefficients into grib-file 'scalw'  | FALSE  |
| LRENORMALIZE   | LOGICAL | Re-normalise initial singular vectors using inner product defined by 'suscal'  | FALSE  |

The routine **SULCZ** defines the constants as listed in Table 2.1 and determines the configuration of the singular vector computation.

optimisation region in the Caribbean is specified ( $0^{\circ} - 25^{\circ}\text{N}$  and  $100^{\circ} - 60^{\circ}\text{W}$ ). The computation of the singular vectors targeted on tropical cyclones uses a diabatic version of the tangent-linear model; i.e. large-scale condensation and cumulus convection are represented in the perturbation model (Barkmeijer *et al.*, 2001; Puri *et al.*, 2001).

The computation is triggered for tropical cyclones between  $40^{\circ}\text{S}-40^{\circ}\text{N}$ . Therefore, the optimisation regions can significantly overlap with the optimisation region of the extra-tropical singular vector computation. In order to avoid a duplication of perturbations present in the subspace of the extra-tropical singular vectors, the singular vectors targeted on a tropical cyclone are computed in the subspace orthogonal to the space spanned by the leading 50 extra-tropical singular vectors (Leutbecher, 2007).

## 2.4 CALCULATION OF INITIAL PERTURBATIONS

The perturbations of the initial conditions are obtained from the singular vectors via a multivariate Gaussian sampling technique described in more detail by Leutbecher and Palmer (2008). Preliminary experimentation with an earlier version of the Gaussian sampling software is reported by Ehrendorfer and Beck (2003).

The generation of the ensemble initial perturbations consists of 6 steps. Task names are given in parentheses.

- (i) retrieval and interpolation from the ECMWF MARS archive of the unperturbed analysis (getini and inidata).
- (ii) retrieval from the ECMWF MARS archive of the estimate of analysis error (getea).
- (iii) singular vector retrieval from the ECMWF ECFS and pre-processing (getsvs).
- (iv) generation of initial perturbations (rot). The initial condition perturbations are written to a grib-file 'pert.grib' and are later archived in MARS (task lag/./archive/icp/ml).
- (v) generation of the perturbed initial conditions at full resolution: spectral expansion and vertical interpolation of initial perturbations, and addition of the initial perturbations to the unperturbed analysis (pert.ic/NNN/pertinic).
- (vi) non-linear integrations starting from unperturbed (cf/control) and perturbed initial conditions (pf/nm); see Section 3.

Hereafter a brief description of each step is given.

## 2.5 UNPERTURBED ANALYSIS RETRIEVAL AND INTERPOLATION

Task (mc/sv/getini) retrieves from the ECMWF MARS archive the unperturbed analysis at full resolution (T799L91). Task (mc/sv/inidata) interpolates the analysis to the resolution of the nonlinear forecasts (T399L62).

## 2.6 ANALYSIS ERROR ESTIMATE RETRIEVAL AND SMOOTHING

This task (mc/sv/getea) retrieves the 4D-Var estimate of analysis error standard deviation from the ECMWF MARS archive. The standard deviation is retrieved on all model levels on a reduced Gaussian grid corresponding to the singular vector resolution. To avoid spuriously small local values of the analysis error standard deviation, the fields are smoothed by truncation to total wavenumber  $\leq 21$ .

## 2.7 GENERATION OF INITIAL PERTURBATIONS

This task (mc/sv/rot) generates the initial perturbations. The relevant shell-script is `sample.svs` in `scripts/gen`. The Gaussian sampling is performed in the following three steps

- (i) Computation of the standard deviation BETA of the sampled Gaussian distribution for each set of singular vectors. This happens by comparing the singular vectors with an estimate of analysis error standard deviation provided by 4D-Var. See program `aev_norm` in `prepdata/mc_tools`.



**Table 2.2** SHELL-variables determining the scaling parameter  $\gamma$  which controls the standard deviation of the sampled Gaussian distribution according to Eq. (2.2).

| $\gamma$                    | singular vector sets        | singular vector files |
|-----------------------------|-----------------------------|-----------------------|
| EPSGAMMA                    | initial extra-tropical SVs  | svifs, svifss         |
| EPSGAMMA * EPSGAMMA_EVO2INI | evolved extra-tropical SVs  | svevo, svevos         |
| EPSGAMMA * EPSGAMMA_TC2INI  | initial SVs targeted on TCs | svifs1, ..., svifs6   |

- (ii) Generation of coefficients for the Gaussian sampling. See program `gen_sv_coeff` in `prepdata/mc_tools`.
- (iii) Linear combination of singular vectors. See program `sv_lin_combi` in `prepdata/mc_tools`.

### 2.7.1 Standard deviation for Gaussian sampling

The scaling of the width of the Gaussian distribution is performed independently for each set of singular vectors. A standard deviation  $\beta$  of the Gaussian distribution to be sampled is determined as follows. The singular vectors are compared with an estimate of the analysis error standard deviation provided by the four-dimensional variational assimilation system using an analysis error variance norm defined as  $L^2$ -norm of the perturbation scaled by the estimate of the analysis error standard deviation. The summation in the norm extends over the entire model grid and involves the horizontal wind components, temperature and the logarithm of surface pressure, i.e. the variables defining the dry model state in grid point space. The standard deviation of the Gaussian for a set of singular vectors is set to

$$\beta = \gamma / \bar{\kappa}, \quad (2.2)$$

where  $\bar{\kappa}$  denotes the average analysis error variance norm for the set of singular vectors. The parameter  $\gamma$  is determined empirically to yield adequate ensemble dispersion. Presently, the EPS uses  $\gamma = 0.014$  for the extra-tropical singular vectors and  $\gamma = 0.021$  for the singular vectors targeted on tropical cyclones.

For the extra-tropical initial singular vectors the scaling factor  $\gamma$  is determined by three SHELL-variables. Table 2.2 describes how  $\gamma$  is set depending on the three variables.

### 2.7.2 Gaussian sampling coefficients

The coefficients for each set of singular vectors are generated by a call to program `gen_sv_coeff`. For each singular vector  $j$  and each odd member  $k$  random coefficients  $\alpha_{jk}$  are drawn from the Gaussian distribution with mean zero and standard deviation  $\beta$ . The coefficients for the even members are set to minus the coefficients of the preceding member, i.e.

$$\alpha_{j\ k+1} = -\alpha_{j\ k}, \quad \text{for } k = 1, 3, 5, \dots \quad (2.3)$$

A Gaussian distribution has no compact support; the coefficients can become arbitrarily large although this is unlikely. In order to avoid numerical instabilities due to excessively large perturbation amplitudes the coefficients are limited to the range  $[-3\beta, +3\beta]$ .

### 2.7.3 Linear combination

The singular vectors are linearly combined using program `sv_lin_combi`. The linear combination is performed in spectral space using the truncation of the singular vector computation. For each set of singular vectors, the singular vectors are read and the previously generated coefficients. The perturbations are written to a single file `pert.grib`. The perturbations are then transferred to the fdb as type=`icp` (initial condition perturbation).

## 2.8 GENERATION OF THE PERTURBED INITIAL CONDITIONS

Task NN/pertinic in family `pert_ic` generates the perturbed initial conditions for member NN at the resolution T399L62 of the first nonlinear integration.



## Chapter 3

# Computational details: non-linear integrations

### Table of contents

- 3.1 Introduction**
- 3.2 Family legA**
  - 3.2.1 Control forecast family legA/fc/cf
  - 3.2.2 Perturbed forecast family legA/fc/pf
  - 3.2.3 Calibration/validation forecast family legA/fc/cv
- 3.3 Family legB**
  - 3.3.1 Control forecast family legB/fc/cf
  - 3.3.2 Perturbed forecast family legB/fc/pf
- 3.4 Family legC**

### 3.1 INTRODUCTION

At the time of revising this documentation (December 2008), the model resolution is T399L62 between forecast day 0 and 10, and T255L62 between forecast day 10 and 15 (or 32 on Thursdays at 00 UTC) – see [Vitart \*et al.\* \(2008\)](#) for a description of the system. The merged VAREPS/monthly system (hereafter simply called the Ensemble Prediction SYstem, EPS) runs twice-a-day, at 00 and 12 UTC, with slightly different configurations:

- 00 UTC: forecasts are run with with persisted SST anomalies from day 0 to day 10, and with coupled ocean model from day 10 to day 15 every day apart for Thursday, when forecasts are extended to day 32.
- 12 UTC: forecasts are run with persisted SST anomalies from day 0 to day 15.

This is the operational configuration since 11 March 2008 (see [Buizza \*et al.\* \(2007\)](#) and [Vitart \*et al.\* \(2008\)](#) for a description of the operational configuration, and [Buizza \*et al.\* \(2003\)](#) for a description of the benefits of increasing the spatial resolution for the EPS).

Since the introduction of the merged VAREPS-monthly EPS on 11 March 2008, each of the 51 15-day non-linear integrations have been performed in tasks grouped in three families, legA, legB and legC. This facilitates the production of the ensemble forecast products in different batches: the first one which includes only products up to forecast day 10, the second one which includes also the 15-day products, and the third one (on Thursdays) which includes also the monthly products. A detailed description of the VAREPS technical implementation, including a detailed discussion on how to retrieve forecast data across the resolution change, can be found in [Buizza \*et al.\* \(2006\)](#).

### 3.2 FAMILY LEGA

Family 'legA' includes the generation of the initial perturbations (see [Section 2.4](#)) and the first 10-day forecast integration. These forecasts are all run with persisted SST anomalies. Under sub-family 'legA/fc', three types of forecasts are currently run: the ensemble control forecast, the ensemble perturbed forecasts and the 2 extra calibration/validation forecasts.

### 3.2.1 Control forecast family legA/fc/cf

The control forecast family includes two tasks: task legA/fc/cf/getinileg copies the initial conditions in the forecast working directory, while task legA/fc/cf/modeleps performs the day 0 to day 10 integration at resolution T399 and with 62 vertical levels. Control forecast data are archived in MARS (the ECMWF Meteorological Archival and Retrieval System) as type 'cf' of stream 'enfo'.

### 3.2.2 Perturbed forecast family legA/fc/pf

This family includes 51 sub-families, named legA/fc/pf/001, legA/fc/pf/002, .... Each sub-family includes the same two tasks as the control forecast: task legA/fc/cf/getinileg copies the perturbed initial conditions in the forecast working directory, while task legA/fc/cf/modeleps performs the day 0 to day 10 integration at resolution T399 and with 62 vertical levels. Perturbed forecast data are archived in MARS as type 'pf' of stream 'enfo'.

### 3.2.3 Calibration/validation forecast family legA/fc/cv

This family includes 2 sub-families, named legA/fc/cv/control\_1 and legA/fc/cv/control\_2: these two sub-families include tasks to run two extra reference forecasts up to 15. These two extra forecasts are performed with constant resolution for calibration and validation purposes (note that these two forecasts are not used to generate any ensemble product). Forecast data from these two calibration/validation forecasts are archived in MARS as type 'cv' of stream 'enfo'. Each sub-family includes the same two tasks as the control forecast: task legA/fc/cf/getinileg copies the perturbed initial conditions in the forecast working directory, while task legA/fc/cf/modeleps performs the 15-day integration, at resolution T399 and with 62 vertical levels for control\_1, and at resolution T255 and with 62 vertical levels for control\_2.

## 3.3 FAMILY LEGB

Under sub-family 'legB/fc', the ensemble control and the perturbed forecasts are extended from forecast day 10 to 15. At 00UTC, these forecasts are run with a coupled ocean model, while at 12UTC the forecasts are run with persisted SST anomalies.

Please note that technically each legB forecast starts from the legA 9-day forecast: when the legB forecast reaches forecast day-1 (which coincides with the legA forecast day-10) its data are archived in MARS as part of the 'enfo' stream. In other words, VAREPS forecast data in MARS stream 'enfo' includes legA T399L62 forecasts from day 0 to day 10, and T255L62 from day 10 to day 15.

### 3.3.1 Control forecast family legB/fc/cf

The control forecast family includes three tasks: task legB/fc/cf/getvarepsdata retrieve all t+9 forecast fields from legA required to start the legB forecast. Task legB/fc/cf/intHtoL interpolates the initial conditions from the legA to the legB resolution. Task legB/fc/cf/modeleps performs the day 9 to day 15 integration at resolution T255 and with 62 vertical levels.

### 3.3.2 Perturbed forecast family legB/fc/pf

This family includes 51 sub-families, named legB/fc/pf/001, legB/fc/pf/002, .... Each sub-family includes the same three tasks as the control forecast: task legB/fc/cf/getvarepsdata retrieve all t+9 forecast fields from legA required to start the legB forecast. Task legB/fc/cf/intHtoL interpolates the initial conditions from the legA to the legB resolution. Task legB/fc/cf/modeleps performs the day 9 to day 15 integration at resolution T255 and with 62 vertical levels.

## 3.4 FAMILY LEGC

Under sub-family 'legC/fc', once-a-week (on Thursdays) the ensemble control and the perturbed forecasts are extended from forecast day 15 to 32 with a coupled ocean model. The ocean model is HOPE, the Hamburg Ocean Primitive Equation model (see [Wolff \*et al.\* \(1997\)](#)), coupled to the atmospheric model through the Ocean Atmosphere Sea Ice Soil (OASIS) coupler with a 3-hour frequency. The ocean initial

conditions come from the near-real-time component of the operational ocean analysis (see [Balmaseda \*et al.\* \(2007\)](#)). For each ensemble member, during LegA (day 0 to 10) the ocean model is forced by the fluxes provided by the atmospheric integration (during this period, the persisted SST anomaly used to force the atmosphere is also used to constrain the SST of the ocean model). More details about the new coupled ensemble can be found in [Vitart \*et al.\* \(2008\)](#).



## References

- Balmaseda, M., Vidard, A. and Anderson, D. (2007). The ECMWF system-3 ocean analysis system. *ECMWF Tech. Memo. No. 508*.
- Barkmeijer, J., Buizza, R., Palmer, T. N., Puri, K. and Mahfouf, J.-F. (2001). Tropical singular vectors computed with linearized diabatic physics. *Q. J. R. Meteorol. Soc.*, **127**, 685–708.
- Barkmeijer, J., van Gijzen, M. and Bouttier, F. (1998). Singular vectors and estimates of the analysis error covariance metric. *Q. J. R. Meteorol. Soc.*, **124**, 1695–1713.
- Bourke, W., Buizza, R. and Naughton, M. (2005). Performance of the ECMWF and the BoM ensemble systems in the southern hemisphere. *Mon. Wea. Rev.*, **132**, 2338–2357.
- Buizza, R. (1994). Localization of optimal perturbations using a projection operator. *Q. J. R. Meteorol. Soc.*, **120**, 1647–1682.
- Buizza, R., Barkmeijer, J., Palmer, T. N. and Richardson, D. S. (1999a). Current status and future developments of the ECMWF ensemble prediction system. *Meteorol. Appl.*, **6**, 1–14.
- Buizza, R., Bidlot, J. R., Wedi, N., Fuentes, M., Hamrud, M., Holt, G., Palmer, T. N. and Vitart, F. (2006). The new ECMWF variable resolution ensemble prediction system (VAREPS): methodology and validation. *ECMWF Tech. Memo. No. 499*.
- Buizza, R., Bidlot, J. R., Wedi, N., Fuentes, M., Hamrud, M., Holt, G. and Vitart, F. (2007). The new ECMWF VAREPS (variable resolution ensemble prediction system). *Q. J. R. Meteorol. Soc.*, **133**, 681–695.
- Buizza, R., Houtekamer, P. L., Toth, Z., Pellerin, G., Wei, M. and Zhu, Y. (2005). A comparison of the ECMWF, MSC and NCEP global ensemble prediction systems. *Mon. Wea. Rev.*, **133**, 1076–1097.
- Buizza, R., Miller, M. and Palmer, T. N. (1999b). Stochastic representation of model uncertainties in the ECMWF ensemble prediction system. *Q. J. R. Meteorol. Soc.*, **125**, 2887–2908.
- Buizza, R. and Palmer, T. N. (1995). The singular vector structure of the atmosphere global circulation. *J. Atmos. Sci.*, **52**, 1434–1456.
- Buizza, R., Petroliaigis, T., Palmer, T. N., Barkmeijer, J., Hamrud, M., Hollingsworth, A., Simmons, A. and Wedi, N. (1998). Impact of model resolution and ensemble size on the performance of an ensemble prediction system. *Q. J. R. Meteorol. Soc.*, **124**, 1935–1960.
- Buizza, R., Richardson, D. S. and Palmer, T. N. (2003). Benefits of increased resolution in the ECMWF ensemble system and comparison with poor-man’s ensembles. *Q. J. R. Meteorol. Soc.*, **129**, 1269–1288.
- Ehrendorfer, M. and Beck, A. (2003). Singular vector-based multivariate normal sampling in ensemble prediction. *ECMWF Tech. Memo. No. 416*.
- Ehrendorfer, M. and Tribbia, J. J. (1997). Optimal prediction of forecast error covariances through singular vectors. *J. Atmos. Sci.*, **53**, 286–313.
- Gelaro, R., Buizza, R., Palmer, T. N. and Klinker, E. (1998). Sensitivity analysis of forecast errors and the construction of optimal perturbations using singular vectors. *J. Atmos. Sci.*, **55**, 1012–1037.

- Golub, G. H. and van Loan, C. F. (1983). *Matrix Computation*. North Oxford Academic Publ. Co. Ltd.
- Hagedorn, R. (2008). Using the ecmwf reforecast dataset to calibrate eps forecasts. *ECMWF Newsletter No. 117*, pp. 8–13.
- Harrison, M. S., Palmer, T. N., Richardson, D. and Buizza, R. (1999). Analysis and model dependencies in medium-range ensembles: two transplant case studies. *Q. J. R. Meteorol. Soc.*, **126**, 2487–2515.
- Hoskins, B. J., Buizza, R. and Badger, J. (2000). The nature of singular vector growth and structure. *Q. J. R. Meteorol. Soc.*, **126**, 1565–1580.
- Houtekamer, P. L., Lefaiivre, L. and Derome, J. (1996a). The RPN ensemble prediction system. In *Proc. ECMWF Seminar on Predictability*, Vol. II, pp. 121–146, 4–8 September 1995, Reading, UK.
- Houtekamer, P. L., Lefaiivre, L., Derome, J., Ritchie, H. and Mitchell, H. L. (1996b). A system simulation approach to ensemble prediction. *Mon. Wea. Rev.*, **124**, 1225–1242.
- Leutbecher, M. (2005). On ensemble prediction using singular vectors started from forecasts. *Mon. Wea. Rev.*, **133**, 3038–3046.
- Leutbecher, M. (2007). On the representation of initial uncertainties with multiple sets of singular vectors optimised for different criteria. *Q. J. R. Meteorol. Soc.*, **133**, 2045–2056.
- Leutbecher, M. and Palmer, T. N. (2008). Ensemble forecasting. *J. Comp. Phys.*, **227**, 3515–3539.
- Molteni, F., Buizza, R., Palmer, T. N. and Petroliagis, T. (1996). The ECMWF Ensemble Prediction System: methodology and validation. *Q. J. R. Meteorol. Soc.*, **122**, 73–119.
- Mureau, F., Molteni, F. and Palmer, T. N. (1993). Ensemble prediction using dynamically conditioned perturbations. *Q. J. R. Meteorol. Soc.*, **199**, 299–298.
- Palmer, R. N., Gelaro, R., Barkmeijer, J. and Buizza, R. (1998). Singular vectors, metrics and adaptive observations. *J. Atmos. Sci.*, **55**, 633–653.
- Palmer, T. N., Molteni, F., Mureau, R., Buizza, R., Chapelet, P. and Tribbia, J. (1993). Ensemble Prediction. In *Proc. of the ECMWF Seminar on Validation of Models over Europe: Vol. 1*, pp. 21–66, 7–11 September 1992, Reading, UK.
- Park, Y.-Y., Buizza, R. and Leutbecher, M. (2008). Tigge: preliminary results on comparing and combining ensembles. *ECMWF Tech. Memo. No. 548*.
- Puri, K., Barkmeijer, J. and Palmer, T. N. (2001). Ensemble prediction of tropical cyclones using targeted diabatic singular vectors. *Q. J. R. Meteorol. Soc.*, **127**, 709–734.
- Rabier, F., Klinker, E., Courtier, P. and Hollingsworth, A. (1996). Sensitivity of forecast errors to initial conditions. *Q. J. R. Meteorol. Soc.*, **122**, 121–150.
- Sleijpen, G. L. G. and van der Vorst, H. A. (1996). A Jacobi–Davidson iteration method for linear eigenvalue problems. *SIAM J. Matrix Anal. Appl.*, **17**, 401–425.
- Terray, L., Sevault, E., Guilyardi, E. and Thual, O. (1995). The oasis coupler user guide version 2.0. *Tech. Rep. CMGC/95-46*, CERFACS, Toulouse.
- Toth, Z. and Kalnay, E. (1993). Ensemble forecasting at NMC: the generation of initial perturbations. *Bull. Am. Meteorol. Soc.*, **74**, 2317–2330.
- Toth, Z. and Kalnay, E. (1997). Ensemble forecasting at NCEP and the breeding method. *Mon. Wea. Rev.*, **125**, 3297–3319.
- Trevisan, A., Pancotti, F. and Molteni, F. (2001). Ensemble prediction in a model with flow regimes. *Q. J. R. Meteorol. Soc.*, **127**, 343–358.
- Vitart, F. (2004). Monthly forecasting at ecmwf. *Mon. Wea. Rev.*, **132**, 2671–2779.



Vitart, F., Buizza, R., Balmaseda, M. A., Balsamo, G., Bidlot, J., Bonet, A., Fuentes, M., Hofstadler, A., Molteni, F. and Palmer, T. N. (2008). The new VAREPS-monthly forecasting system: a first step towards seamless prediction. *Q. J. R. Meteorol. Soc.*, **134**, 1789–1799.

Wolff, O., Maier-Raimer, E. and Legutke, L. (1997). The hamburg ocean primitive equation model. *Tech. Rep. 13*, Deutsches Klimarechenzentrum, Hamburg.